24th EUROPEAN ROTORCRAFT FORUM
Marseilles, France -15th-17th September 1998

HELICOPTER MODEL TESTS - LOAD DIFFERENCES DUE TO WIND TUNNEL TEST SECTION CONFIGURATIONS AND MODEL MOUNTING

Hans-Jürgen Langer
Deutsches Zentrum für Luft-und Raumfahrt e.V. (DLR)
Institut für Flugmechanik
Braunschweig, Germany

Zhang, Zhen Fang & Chen, Wen Xuan
Chinese Helicopter Research&Development Institute (CHRDI)
Jindezhen, Jiangxi, China

Yang, Yong Dong
China Aerodynamics Research&Development Center (CARDC)
Mianyang, Sichuan, China

Référence : TE12

ABSTRACT

Extensive rotor and fuselage tests were performed in two different wind tunnels: The German Dutch Wind Tunnel (DNW) and the Large Low Speed Wind Tunnel at CARDC. In addition, the DNW tests were accomplished for different test section configurations.

The models used were 40%-scaled models of the Bo105. In order to compare with full scale rotor data, the model rotor was operated at full-scale blade tip Mach number (Mach-scaled).
Both wind tunnels feature a closed 8m by 6m test section.

The rotor/fuselage tests in DNW were made in five test section configurations:

- 6m by 6m closed
- 8m by 6m closed
- 8m by 6m closed with 12% open slots
- 8m by 6m open jet
- 9.5m by 9.5m closed

These data along with the CARDC data were used to point out the different measured loads caused by wall interference and model mounting.

It has been shown that not only rotor loads are influenced by wind tunnel wall interference, fuselage loads are affected, too.

As known from classic publications [1], load differences due to test section interference are more significant for higher rotor thrust conditions, but nearly independent with tunnel speed.

Applying calculations and derivative measurements it is possible to compensate wall interference with respect to rotor loads, but this depends highly on code precision and test condition.

At low wind tunnel speed, fuselage loads are mainly influenced by the location of the rotor downwash. This is dependent on the effective rotor angle of attack which varies for the different test sections if wall interference is considered. There is no way to compensate this effect by model adjustments as it is applicable for the rotor only.

NOMENCLATURE

AoA	angle of attack
A_{ro}	rotor disk area, m^2
A_{TS}	test section area, m^2
c_T	rotor thrust coefficient
Ma_{tip}	rotor tip Ma-number @ ISA (=0.641)
$M_{\beta,1p}$	1/rev blade flap moment, Nm
M_x, M_y	rotor rolling, pitching moment, Nm
r	sectional radius, m
R	rotor radius (=2m)
s	scale factor (=2.46 or ≈ 40%)
V	tunnel speed, m/s
v_{tip}	blade tip speed (=216ms^{-1} @ ISA)
$\Delta u, \Delta v, \Delta w$	velocity due to test section boundaries
x,y,z	rotor shaft fixed coordinates (+z down)
α, α_{shalt}	rotor shaft tilt, deg
α_{FT}	rotor shaft tilt from flight tests, deg
α_{sting}	pitch angle of DNW sting support, deg
$\Delta\alpha$	correction angle or derivative
δ_W	wall or boundary correction factor
Ω	rotor rotational speed @ ISA(=110 s^{-1})

Presented at the 24th European Rotorcraft Forum, Marseille, France, September 15 -17, 1998

INTRODUCTION

The use of wind tunnel test measurements plays a significant role in the development of helicopters and for the improvement of prediction codes. However, this is mainly limited to helicopter sub-components like optimisation of fuselage, airfoil investigations, blade load characteristic, etc.
Research related rotor investigations are more common for studies in wind tunnels, e.g. for noise prediction and performance.

Fixed wing wind tunnel investigations are widely common and those models spent much more time in wind tunnel than helicopter models.
Apart from cost aspects the reason is quite clear: The lack of a reliable correction procedure, individually adapted to the used test section size and shape.
Up to now for helicopters there exists no code to calculate the test section flow distortion (Δu, Δv, Δw) based on wall pressure measurements like it is standard for fixed wing corrections.
In order to start filling the gap, DLR and DNW conducted a test program which yielded a good data base about the qualitative and quantitative magnitude of the necessary corrections.
This paper presents the results of DNW tests from mainly three different test section configurations: 1) 8m by 6m open jet, 2) 8m by 6m closed with 12% open slots, and 3) 8m by 6m closed.

An identical test matrix was measured in the 8m by 6m closed test section of CARDC. Since both, the rotor and fuselage, are a 40%-scaled Bo105, it can be expected, that the results fit properly together.

TEST SET-UP

DLR/DNW Wind Tunnel Model

The DNW wind tunnel model is based on the so-called Modular Wind Tunnel Model (MWM). The capabilities of the MWM were described in detail in [2].
Since the MWM is just a basis module for rotor specific measurements, additional hardware was added in order to measure fuselage loads. Beside the *rotor* balance, a 6-component *fuselage* balance measures the total forces and moments with respect to the scaled-down c/g-position of the Bo105.
It can be seen from **fig.1** that a tail rotor is not installed, however, fuselage, skids, and stabiliser are properly scaled. The tail rotor is represented by a dummy stub which has approximately the same drag as the down-scaled original one.
The model rotor was operated at the same tip Mach number as the full scale rotor.
The model was mounted on the DNW sting support which remotely allows vertical (z-position) and α adjustments. The rotor hub of the model was centred at z=3.634m above the test section floor, which is above the wind tunnel centreline with respect to the 8m by 6m test section.
For α_{shaft}=0° the fuselage incidence is +3° (nose-up tilt).
The mounting location was at the aft body below the tail boom (see fig.1).
The influence of mounting can have an impact on fuselage loads. This will be shown when the DNW and CARDC fuselage data are compared.
Operation of the model was done by a joint DLR-DNW team. The DLR team operated the rotor while the DNW was responsible for flow speed adjustment, α_{sting} control and acquisition of pressure signals.

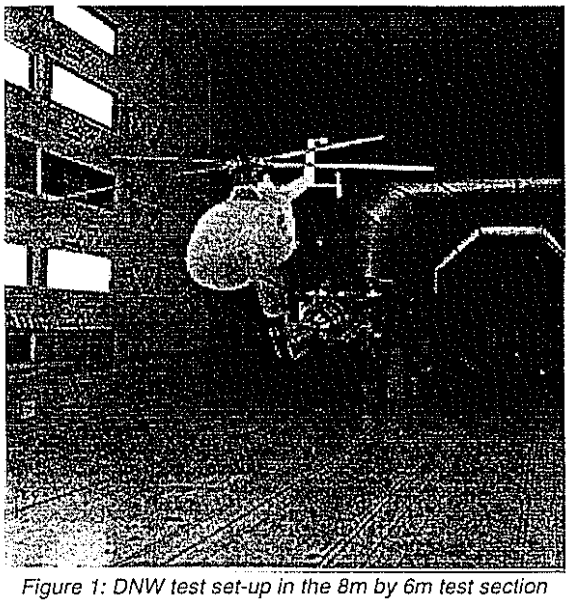

Figure 1: DNW test set-up in the 8m by 6m test section

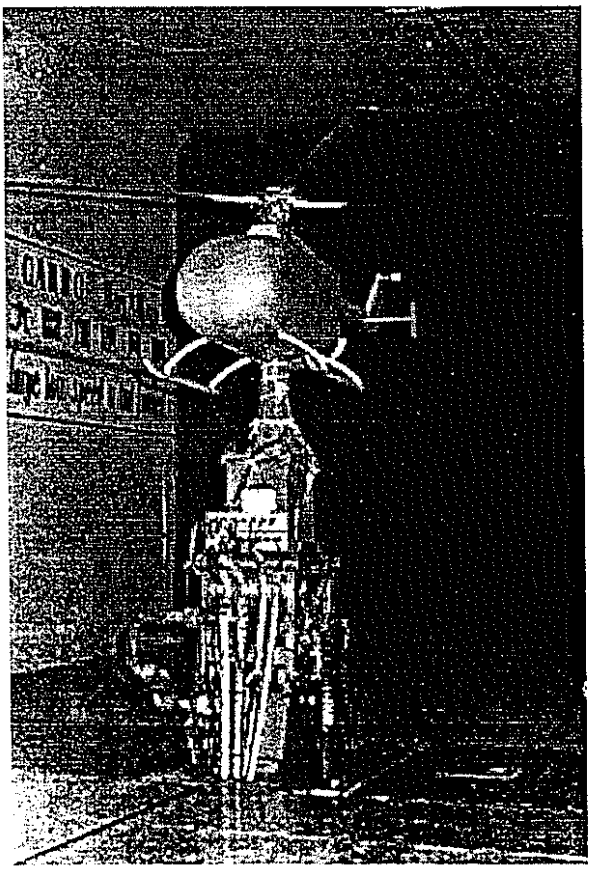

Figure 2: CARDC test set-up in the 8m by 6m test section

CHRDI/CARDC Wind Tunnel Model

Fig. 2 shows the wind tunnel model tested in the 8m by 6m wind tunnel of CARDC. Fuselage and rotor are scaled from the Bo105 - with the same scaling factor (s=2.46) as applied to the DLR model.

The motivation using the same model and size as the DLR model was the unique possibility to correlate measurement results between different wind tunnels. In addition, the models are a good tool to check the accuracy of the measuring system.

As for the DLR model, the fuselage had an built-in tilt back of 3° with respect to the rotor shaft.
The hub position was 3.4m above wind tunnel floor for α=0°. Since the α-hinge had a distance of 2.751m from the rotor hub, the hub center leaves the reference position when the shaft tilts. However, for small α's (as controlled within the test matrix) this should have no impact on the compared results with the DLR model.

MODEL DATA

Basic Technical Rotor Data

Table 1 shows the main rotor data for both rotors:

rotor radius, m	2.0
nominal rotor speed, rpm	1040
blade chord (rectangular), m	0.121
blade twist, deg/m	$6.23^{\pm 0.25}$, r≥0.44m
blade profile	NACA 23012 mod.
contour tolerance,mm	±0.1
design thrust, N	3630
max. thrust, N	8500
blade number	4

Table 1: Basic rotor data

Differences between CARDC and DNW Model configurations

Although model coincidence is widely achieved, some differences should be pointed out:

⇨ wind tunnel:
DNW and CARDC follow different principles of wind tunnel design [3]. The DNW features a 320m long closed flow circuit (principle of Eiffel), while the CARDC tunnel has an open pipe which is about 237m long.
Depending on outside wind and temperature, zero flow speed for hover tests can sometimes not be guaranteed.
The CARDC tunnel is located about 570m above SL, therefore data correlation was made with reference to ISA.

⇨ model mounting:
From **fig. 1** and **fig. 2** the difference of test rig mounting can easily be seen. In order to quantify the differences, some tests were run with rotor blades removed. Results are presented in section "DNW/CARDC Fuselage Data Correlation"

⇨ Blade characteristic:
Due to different requirements concerning blade sensor equipment, the rotors were produced by two companies: The CHRDI rotor were manufactured by the former company MBB[1]. The DLR rotor came from DEI[2].

For the CHRDI rotor, strain gauge sensors are located on the blade skin and mainly within the blade's root area (flap, lag, torsion).

For the DLR rotor, the reference blade featured 34 strain gauge sensors (14 in flap, 12 in lag, and 8 in torsion direction). Three blades had a 'standard' sensor equipment like the CHRDI rotor blades. All sensors were located under the blade skin.

Table 2 shows differences of natural frequencies as a result of different blade properties shown in **fig. 3 to fig. 6.** These figures are results from DEI and MBB calculations.

The figures show that the stiffness differences mainly exists in the blade root area between both blade sets: The CHRDI rotor is stiffer than the DLR rotor.

mode	*CHRDI [1)]*	*DLR [2)]*
1st flap	19.6 (1.12)	19.8 (1.13)
2nd flap	50.3 (2.87)	49.6 (2.83)
3rd flap	90.5 (5.17)	87.6 (5.01)
1st chordwise	13.7 (0.78)	14.1 (0.81)
2nd chordwise	78.9 (4.51)	91.8 (5.25)
1st torsional	70 (4.00)	61.8 (3.53)

Table 2: Natural frequencies in Hz and (n/rev) at 1050rpm [1)] Data from MBB, [2)] Data from DEI

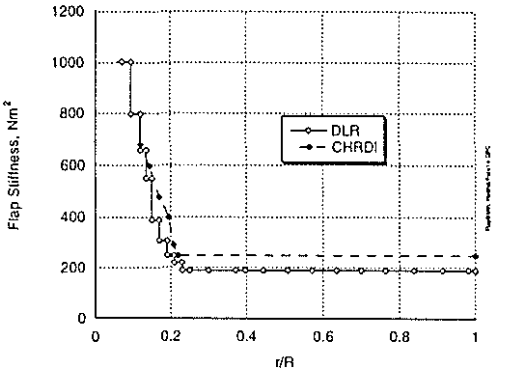

Figure 3: Blade Stiffness of DLR and CHRDI rotor in flap direction

Although the DLR blade has two additional masses along blade span (fig. 6) and lower stiffness, the 1st order natural frequencies in flap and lag are higher. It can be assumed that the used calculation tools do not yield comparable results.
The torsion stiffness of the CARDC blade is much higher which reflects, too, the 1st torsion natural

[1] now ECD
[2] Dynamic Engineering Inc.

frequency. This has an impact on rotor coning and effective twist along blade span.

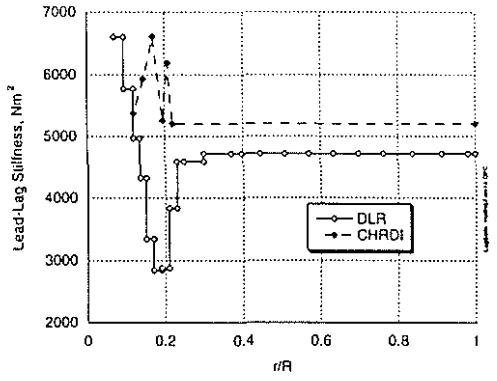

Figure 4: Blade Stiffness of DLR and CHRDI rotor in lead-lag direction

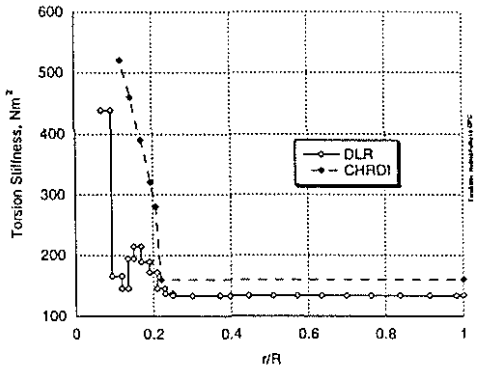

Figure 5: Blade Stiffness of DLR and CHRDI rotor in torsion

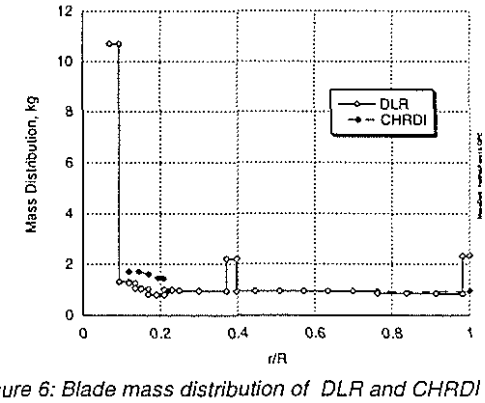

Figure 6: Blade mass distribution of DLR and CHRDI rotor

TEST PROGRAM

The wind tunnel program in the DNW and CARDC (8x6m closed test section only) was tailored to six different tasks:

1) Correlation with flight tests;
   Sections tested: 6x6m closed, 8x6m closed, 8x6m open, 9.5x9.5m closed

2) Rotor trim to power from flight test;
   Sections tested: 6x6m closed, 8x6m closed, 8x6m 12% slotted, 8x6m open, 9.5x9.5m closed

3) Minimised flap bending moment trim to zero α_{shaft};
   Sections tested: 6x6m closed, 8x6m closed, 8x6m 12% slotted, 8x6m open, 9.5x9.5m closed

4) Hover tests, correlation with flight tests;
   Sections tested: 6x6m closed, 8x6m closed, 8x6m open

5) Derivatives;
   Sections tested: 6x6m closed, 8x6m closed, 8x6m open, 9.5x9.5m closed (one speed only)

6) Fuselage only (blades and/or shaft removed);
   Sections tested: 6x6m closed (DNW), 8x6m closed (CARDC)

Tests with minimized flap bending trim at zero shaft angle (task 3) were accomplished to identify trim differences between the models in the DNW and CARDC. Since the model control is well defined, data correlation between both configurations requires no interpolation.

The hover tests (task 4) were performed at α_{shaft}=-20° (-15° CARDC) in the closed test sections and at 0° in the open test section.

The derivative measurements in task 5 are an essential tool if interpolation is necessary between measured results.
Since the derivative elements (e.g., $\Delta c_T/\Delta\alpha$) are assumed to be linear in a small α-range only, the use of derivatives for extrapolation is often not accurate enough.

For the most important parameters (e.g., thrust, rotor speed, etc.) the rotor was trimmed to non-dimensional parameters in order to compensate the density influence.

In all but the open test section, DNW personnel acquired wall pressure measurements using 92 pressure sensors. The sensors were installed along the floor (3 rows), along the side walls (2 rows each), and along the ceiling (3 rows).
Preliminary signal analysis of the pressure sensors shows that the flow has strong gradients and has no symmetry. An in-depth signal analysis has not been performed yet.

RESULTS

Results are presented twofold:

⇨ DNW - CARDC data correlation:
Results from the 8m by 6m closed test section only.

⇨ DNW test section correlation:
Discussion of measurement results from rotor and fuselage from the different test sections of the DNW.

DNW/CARDC Fuselage Data Correlation

a) Blades Off

Fuselage data are obtained from a 6-component fuselage balance which is calibrated to measure wind loads only. The fuselage has a 3° 'nose-up' built-in tilt with respect to the rotor shaft.
Even for those tests where the shaft was removed (see section 'Test Program', task 6) measurements are done with a 3° fuselage tilt back.
Figure 7 shows the fuselage drag and lift for removed blades. The drag is exactly that what was calculated for the scaled down Bo105.
The drag difference between CARDC and DNW fuselage is small and can be explained by fuselage - support interference.
The difference in z-direction is likely caused by the position and interference of the model mount. It can be assumed that the flow behind the DNW model support (see fig.1) have a strong pressure gradient which has an impact on the empennage loads.

Reference [4] explains differences from sting interference measurements on *tailplane* pressure distribution for *fixed wing models*. For sting-mounted models the normal force is mainly influenced depending on Mach number and shape of the sting.
Since pressure measurements close to the model support are not available - neither for the DNW nor for the CARDC - quantifying the interference effect is not possible.
A certain effect on lift also may have the fairing (cover plate) between fuselage and rotor shaft which was not used for the CARDC tests.

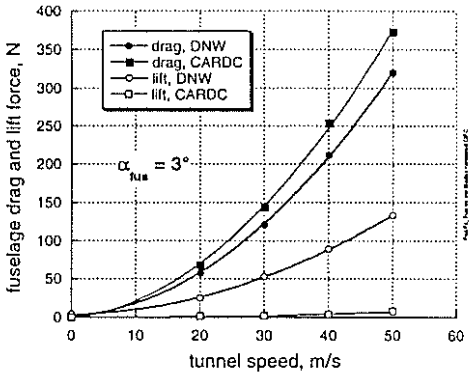

*Figure 7: **Fuselage** forces in x and z; blades removed*

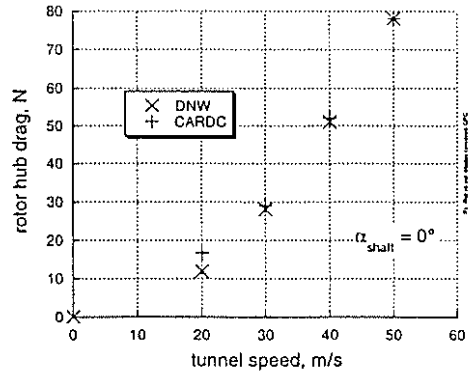

*Figure 8: **Hub** force in x-direction; blades removed*

In **fig. 8** the rotor hub drag force is plotted versus wind tunnel speed. The drag force (=-F_x for α_{shaft}=0°) is measured via the 6-component *rotor* balance.

Since the curves widely collapse for DNW and CARDC, the conclusion can be drawn that (1) model mounting has no impact on *rotor hub* loads, and (2) cables and the data distribution box, located on the hub, is widely similar in its shape between CARDC and DNW model.

b) Blades On

After the blades had been attached to the rotor hub, it is of interest to correlate the fuselage force loads between the DNW and CARDC model for the spinning rotor.

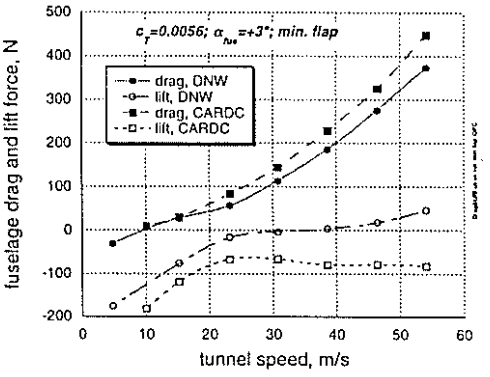

Figure 9: Influence of rotor downwash on fuselage loads

As expected the curves in **figure 9** are slightly different compared to fig. 7. The lift negative at small speeds which means fuselage download due to rotor downwash.

Apart from lower speeds (v<30m/s) where the flow through the rotor hits the fuselage, the curves are quite similar, but show a certain shift with respect to fig. 7. This is caused by the rotor position with respect to the tunnel centreline and by the lift of the rotor disk deflecting the total flow downwards in the test section within and behind the rotor area.

DNW/CARDC Rotor Data Correlation

After having correlated fuselage loads between CARDC and DNW measurements, it is of interest how the *rotor* data fits together.
Results from hover tests can be used to find out whether blade deviations - mainly the torsion stiffness (see section 'Model Data') - influence rotor power, since torsion stiffness has an impact on the local blade twist. It is known that with increasing blade twist, the consumed power decrease (with the drawback of higher vibration): **Fig. 10** shows nothing at all.
The only - but small - difference is visible between open and closed DNW curves which is likely due to ground effect.
The *closed* DNW tests were made at α_{shaft}=-20° (CARDC tests at α_{shaft}=-15°) and for the *open* jet tests, the rotor disk was about 12m above ground.

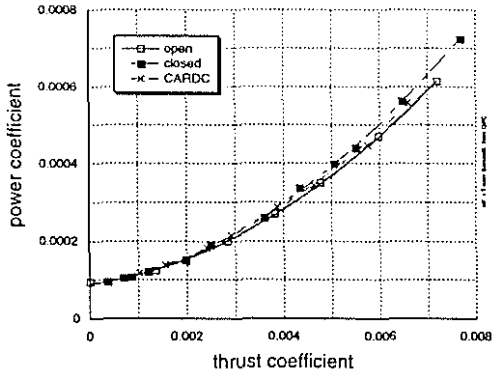

Figure 10: Hover tests from three 8x6m test sections

The high rotor angle of attack accelerates the total flow within the closed tunnel. This produced a u-shape vortex on the test section floor bound with a drop in pressure. This results in a slightly higher power consumption for the same thrust.

The non-dimensional power versus wind tunnel speed is plotted in **Fig. 11** for both models. Each pair of curves represent a different rotor trim condition. The curves with the filled symbols show flight test trim conditions, i.e. $M_{\beta,1p} \neq 0$.

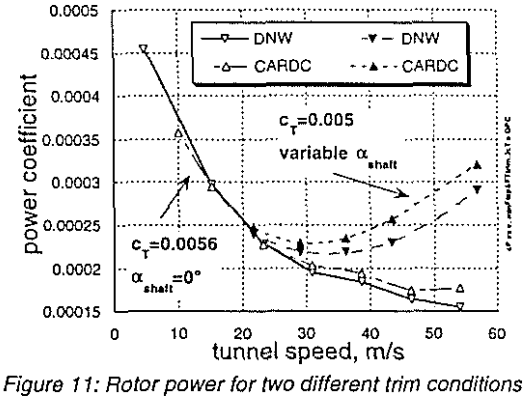

Figure 11: Rotor power for two different trim conditions

For the curves with the open symbols the mast bending moments were zero, the rotor trim was at slightly higher thrust, and shaft tilt was zero, too.

Apart from the low speed region, where the curves fit properly, the medium and high speed region shows some differences whereas the CARDC rotor consumes more power than the DNW rotor.

The reason for that is assumed to be a difference in AoA of the rotor plane which can be caused either by model support interference or - more likely - by rotor moment trim.

From [5] it is known that the mast moment trim, which is directly linked to the rotor plane AoA, has a strong impact on rotor power.

The CARDC tests had used the M_x and M_y of the rotor *balance* to trim the rotor while DNW rotor was trimmed to 1p *mast bending* moment, so small differences can be assumed.
However, it seems more likely that the effective AoA is different between both models. For the DNW curve, it needs just 1.3° more tilt in α_{shaft} to get coincidence (see **fig. 12**).

Static derivatives can often be used to determine rotor control effectiveness and are good for interpolation or even extrapolation between data points.
Derivatives are defined as small variations (e.g. of rotor control angles) around a baseline data point (reference condition). If a non-linear response is expected, *extrapolation* can lead to misleading results.

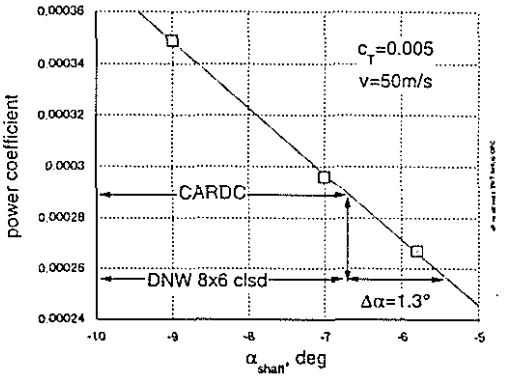

Figure 12: α-correction for DNW-CARDC coincidence

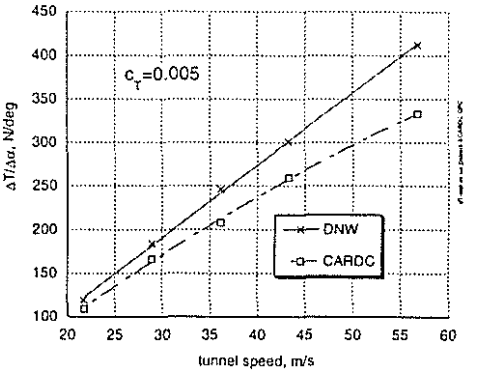

Figure 13: Thrust shift due to α_{shaft} change

Fig.13 shows the thrust change for α_{shaft}-variations versus tunnel speed. The difference between DNW and CARDC curve is due to the different reference condition, likely caused by a different effective rotor AoA as explained for fig. 11.

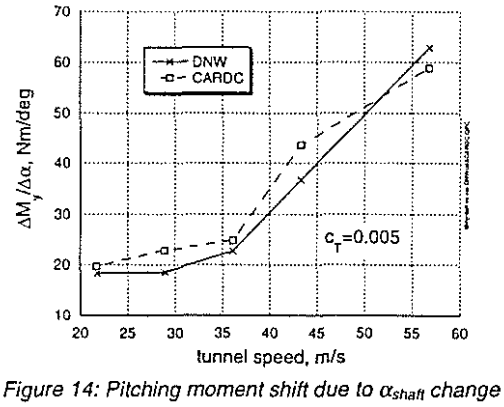

Figure 14: Pitching moment shift due to α_{shaft} change

Although there is some more scatter in the curves, **Fig. 14** shows much better coincidence between DNW and CARDC measurements.
This is due to the smaller impact of α on the pitching moment because having the same baseline condition is of minor importance between CARDC and DNW.

This can also be seen in **Fig. 15**, where the thrust over speed derivative is plotted.

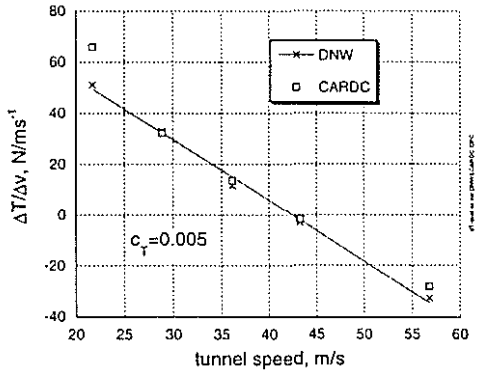

Figure 15: Thrust shift due speed change

DNW Results from Different Test Sections

Results from the 8m by 6m test sections of the DNW often show that load and/or control differences are important depending on test section configuration. Results from the open, closed, and closed with open slots (12% of the total area) test sections are presented here.

Fuselage Pitching Moment

Considering the speed envelope of a helicopter, there is an area where the flow through the rotor hits the empennage and stabiliser. As soon as the helicopter operates in this speed range, the fuselage reaction is a nose-up pitching moment.
Wind tunnel investigations on the pitch-up behaviour are important within the design phase of a helicopter. Location and size of the stabiliser can be optimized in order to reduce the pitch-up moment or to shift it to a desired speed range.
Although transferability of the results from the model to the full scale helicopter is often questioned, results presented here, give confidence.

Note: The moments must be multiplied by s^3 to get the full scale values.

The following five figures (**fig. 16 to fig.20**) gives an impression of the pitch-up effect the helicopter suffers when in transition. A positive moment means nose-up.

In **fig. 20** the α_{shaft} and blade 1p-flap were varied with speed, dependent on measured flight conditions.

Each plot shows a *different thrust* which has an effect on the magnitude of the pitch-up moment, but has just a small impact on the pitching moment at higher speed i.e. v>30m/s.

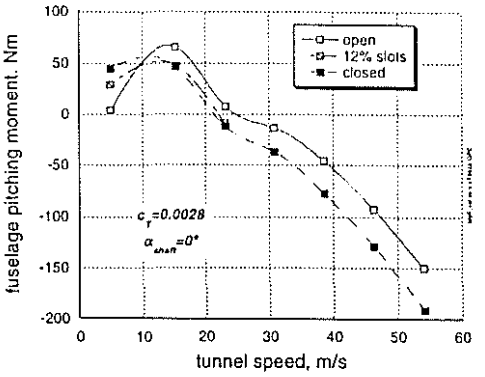

Figure 16: Fuselage pitching moment w.r.t. full scale c/g at c_T=0.0028; rotor trim to minimum flap

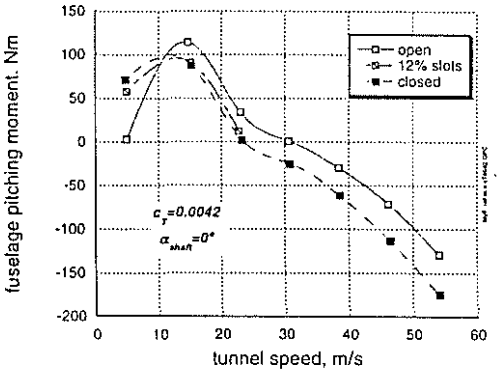

Figure 17: Fuselage pitching moment w.r.t. full scale c/g at c_T=0.0042; rotor trim to minimum flap

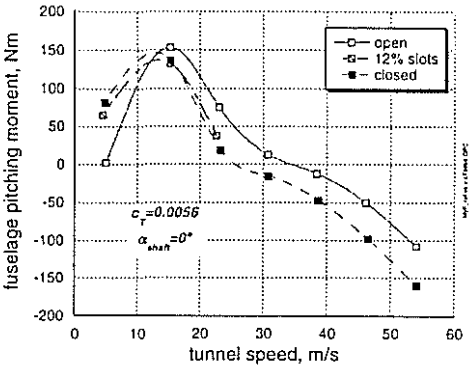

Figure 18: Fuselage pitching moment w.r.t. full scale c/g at c_T=0.0056; rotor trim to minimum flap

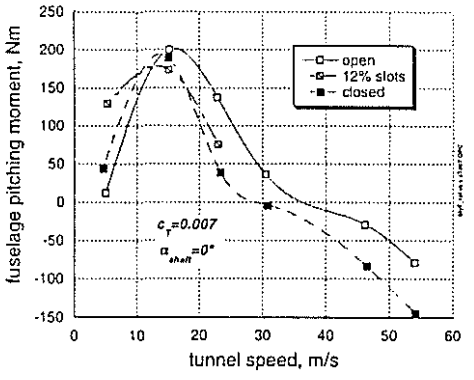

Figure 19: Fuselage pitching moment w.r.t. full scale c/g at c_T=0.007; rotor trim to minimum flap

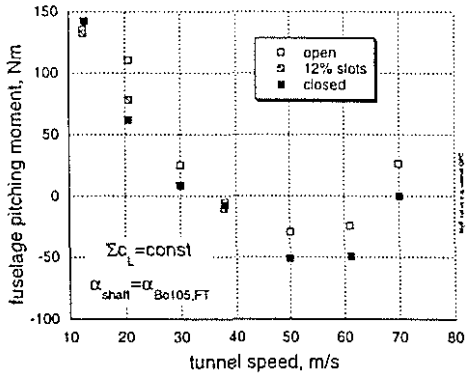

*Figure 20: Fuselage pitching moment w.r.t. full scale c/g for total c_L=0.005; rotor **trim to flight test** conditions*

This shows that the flow dominates generated by wind tunnel rather than the rotor downwash. However, the latter has still a certain influence on the fuselage moment for the highest c_T (fig. 19).

For speeds higher than 30m/s the fuselage shows less nose down moment in the closed test section and more moment in the open jet.

Although the number of data points are small around the curve peaks, the maxima can properly be identified.
As expected, the lower the thrust the smoother the peak. The test section specific interference is nearly constant for speeds beyond 30m/s. This indicates that a general AoA difference exists between the open and closed test section.

The transition between nose up and nose down moment is dependent on the thrust but is for all conditions around 30m/s (0.1<μ<0.15).

It is of interest that the wall interference has just a small impact on the maximum pitch-up moment but more on speed: The open jet maximum moment is always higher than for the closed or slotted test section. This is due to the α-correction of the rotor which must be applied for the different test sections. In [5] it was proven that the slotted walls configuration needs nearly no α-correction with respect to rotor loads. Therefore these curves can directly be applied to the full-scale helicopter with sufficient accuracy.

The test section interference seems to be most effective before and after the maximum pitch up moment has been reached, i.e. at about μ=0.025 and μ=0.1 - even independent on trim condition. This is surprising because the wall interference theory says that the lower the speed the stronger the wall effect. For the low speed the theory seems to be valid, however, not for the values beyond the maxima.

It is assumed that two effects collapse: On the one hand the decreasing rotor/ fuselage interference with advancing speed and on the other hand the increasing α-derivative, which means that - with advancing speed - a small α-variation produce stronger reactions on the rotor and fuselage loads.

Except for the highest c_T (fig. 19) the moments for the slotted wall configuration are always between the closed and open jet which makes sense.

Measurements for the highest C_T (see fig. 19) at 5m/s tunnel speed couldn't properly adjusted due to an unstable tunnel flow i.e. stream fluctuations due to high rotor downwash velocities.
Data points at 5m/s show generally higher loads for the closed configuration which is vice versa beyond the curve maxima. In addition, the curves maxima are less distinct for the closed configurations. This can be explained by the much higher flow disturbance at very low speed because the rotor takes the flow from the wind tunnel only, while the rotor in the open jet gets air from outside, too.

Control Angles

In order to evaluate how strong test section interference is on the rotor, not only loads should be examined, rotor control angles like collective, longitudinal, and lateral cyclic are of interest, too, because rotor trim calculations are widely based on control data input.

For a constant c_T and zero mast bending moment **figures 21 to 23** show the rotor control angles as measured at the blade root pitch hinge. The sensor signal, measured in the time domain, was transformed in the frequency domain where the zero and 1p parts are filtered out.

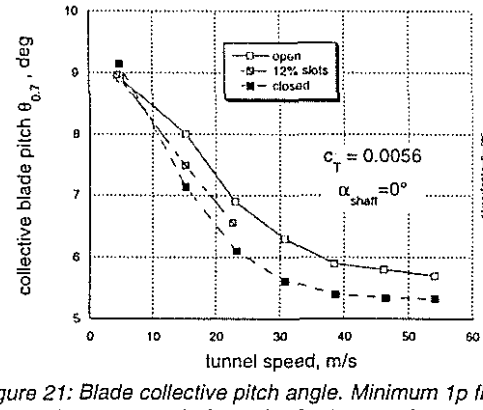

Figure 21: Blade collective pitch angle. Minimum 1p flap trim at zero degree rotor shaft. 8m by 6m test sections

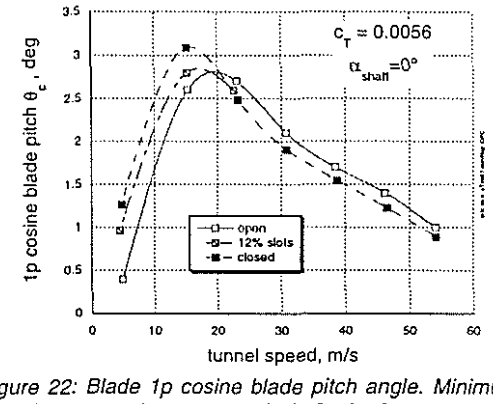

Figure 22: Blade 1p cosine blade pitch angle. Minimum 1p flap trim at zero degree rotor shaft. 8m by 6m test sections

The control angles show what the theory yields when the rotor shaft is kept constant with speed: The decrease in collective with a maximum at hover, the nearly linear increase of $|\theta_s|$, and the classical shape

of θ_c, which demands a detailed mathematical rotor downwash model for good correlation with measured data.

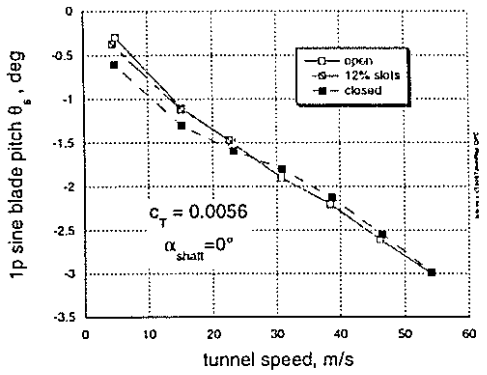

Figure 23: Blade 1p sine blade pitch angle. Minimum 1p flap trim at zero degree rotor shaft. 8m by 6m test sections

Apart from 1p-sine blade pitch (fig. 23) all results show a significant difference between the test sections used, whereas the collective pitch (fig.21) shows the strongest influence. With close to one degree around 20m/s between the open and closed test section wall interference cannot be neglected and must be considered for code validation.

Figure 24 shows the wall corrected collective blade pitch angle.
A criterion for the correction quality is, that the curves to be corrected must collapse after the correction was applied.
Since it is not possible to apply the α-correction directly to the collective, a procedure was chosen which provides excellent results.

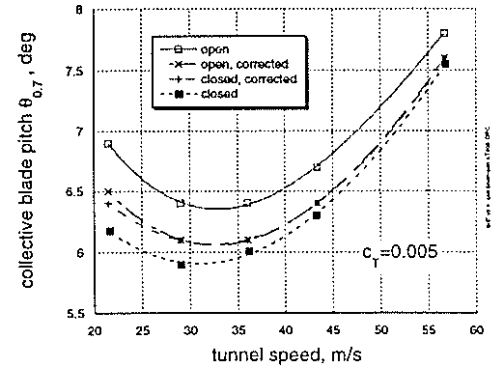

Figure 24: α-corrected and non-corrected collective blade pitch angles. Minimum 1p flap trim.

The correction applied initially was the Glauert formula explained in detail in [5].

$$\Delta\alpha = \frac{180}{\pi} \times \left[\frac{2\delta_W c_T A_{ro} v_{tip}^2}{V^2 A_{TS}} \right] \quad [\text{deg}]$$

with

$$\Delta\alpha = \alpha_{FT} - \alpha_{shaft}$$

Results of the calculated α_{shaft} corrections are plotted in **figure 25.**

After the α-correction values were determined, the *derivative* measurements are used to find the corrected control angle $\theta_{0.7}$.
Derivative measurements are performed in the open and closed test section for the same speed and c_T as those in fig. 24 with the only difference that 1p flap was non-zero.
The measured derivative coefficients along with the corrected α's, and mast moment differences, yield a $\Delta\theta_{0.7}$ which is added to the $\theta_{0.7}$ of the baseline run where the derivatives are built around. The result is a corrected $\theta_{0.7}$ either for the open or for the closed test section.

As can be seen from fig. 24, the method to combine the classical wall correction method with measured derivatives can well be used for control angle correction.

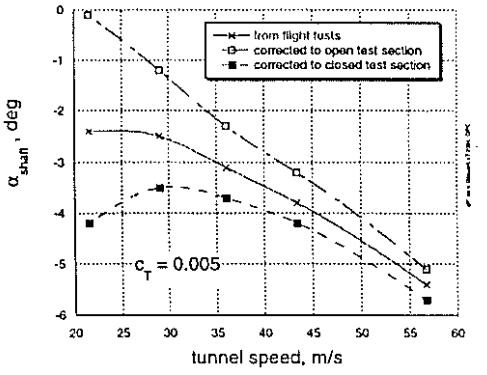

*Figure 25: α-correction due to wall effect. Minimum 1p flap trim. δ_W=0.119 (closed 8*6m) and δ_W=-0.158 (open 8*6m)*

Comparing fig. 24 and fig. 21, it can be seen that the slotted test section can be used, too, to minimize corrections, since the 12%-slot curve matches well to the corrected $\theta_{0.7}$ curve.

CONCLUDING REMARKS

This paper presents results from correlation measurements from two different wind tunnels - DNW and CARDC 8mx6m closed test section. In addition, measurements are shown from the open and slotted wall test section of the DNW. The models used featured a 40% scaled Bo105 rotor and fuselage. Apart from the model mounting - the models are nearly identical. Small differences can be found in the blade properties which has a small effect on the considered fuselage and rotor data.

The following conclusions can be drawn:

a) DNW-CARDC comparison of results

- Fuselage lift and drag is influenced by model mounting and fairing which have only negligible effect on rotor hub loads. Detailed tests - esp. wall pressure tests - are necessary to quantify the influence.
- With the presence of rotor downwash, the fuselage lift and drag is dependent on the model's

vertical position with respect to the tunnel centerline.

- Rotor moment trim has a strong impact on rotor power since it directly influences the total AoA.
- Good coincidence of derivative measurements can be found for those derivatives where the baseline condition trim is of minor importance.

b) DNW test section comparison

- The test section configuration has a strong effect on the fuselage pitch-up curve shape vs. tunnel speed.
- The effect and magnitude of fuselage pitch-up characteristics can well be investigated in the wind tunnel. Negligible corrections are necessary when measured in the 'slotted walls' configuration.
- The test section wall configuration has just a small impact on the maximum pitch-up moment, but has an influence on its location with respect to tunnel speed.
- Wall interference is obvious when rotor control angles are compared. Mainly collective is effected. The classical Glauert α-correction bound with derivative measurements can effectively be used to compensate wall effects.
- Post data processing to eliminate wall interference effects, can be avoided, when the 12% slotted wall test section is used.

ACKNOWLEDGEMENT

The authors wish to thank all those whom invaluable assistance contributed to the success of the programs: The colleagues from CHRDI, CARDC, DNW, and DLR.

REFERENCES

[1] Pope, Alan, and Harper, John J., Low-Speed Wind Tunnel Testing, John Wiley & Sons, Inc., 1966.

[2] Stephan, M., Klöppel, V., and Langer, H. -J., "A New Test Rig For Helicopter Testing," Proceedings of the Fourteenth European Rotorcraft Forum, Milan, Italy, 1988.

[3] Langer, H.-J., Zhang, Z.F., Shen, L.: Results from a Rotor Data Correlation Program Performed in the CARDC and DNW Wind Tunnels. DLR IB 111-93/31, 1993

[4] Carter,E.C.: Interference Effects of Model Support Systems. AGARD-Report No. 601 on Problems in Wind Tunnel Testing Technique; April 1973

[5] Langer, H.J., Peterson R.L., Maier, T.H.: An Experimental Evaluation of Wind Tunnel Wall Correction Methods for Helicopter Performance. 52nd AHS, Washington D.C. June 4-6,1996